(This is a sample cover image for this issue. The actual cover is not yet available at this time.)

Journal of Nuclear Materials 433 (2013) 160–166

Contents lists available at SciVerse ScienceDirect

Journal of Nuclear Materials

journal homepage: www.elsevier.com/locate/jnucmat

A high burnup model developed for the DIONISIO code

A. Soba [a], A. Denis [a,*], L. Romero [b], E. Villarino [c], F. Sardella [c]

[a] U.A. Combustibles Nucleares, Comisión Nacional de Energía Atómica, Avenida del Libertador 8250, 1429 Buenos Aires, Argentina
[b] U.A. Reactores Nucleares, Comisión Nacional de Energía Atómica, Avenida del Libertador 8250, 1429 Buenos Aires, Argentina
[c] Departamento Ingeniería Nuclear, INVAP SE, Comandante Luis Piedra Buena 4950, 8430 San Carlos de Bariloche, Río Negro, Argentina

ARTICLE INFO

Article history:
Received 19 March 2012
Accepted 11 August 2012
Available online 21 September 2012

ABSTRACT

A group of subroutines, designed to extend the application range of the fuel performance code DIONISIO to high burn up, has recently been included in the code. The new calculation tools, which are tuned for UO_2 fuels in LWR conditions, predict the radial distribution of power density, burnup, and concentration of diverse nuclides within the pellet. The balance equations of all the isotopes involved in the fission process are solved in a simplified manner, and the one-group effective cross sections of all of them are obtained as functions of the radial position in the pellet, burnup, and enrichment in ^{235}U.

In this work, the subroutines are described and the results of the simulations performed with DIONISIO are presented. The good agreement with the data provided in the FUMEX II/III NEA data bank can be easily recognized.

1. Introduction

When the residence time of nuclear fuel rods of uranium (or uranium–plutonium) oxide is increased beyond a given threshold value, several properties of the pellet material suffer changes and hence the posterior behavior of the rod is significantly altered. Structural modifications start at the pellet periphery, which is usually referred to as *rim zone*, and are a consequence of the localized absorption of epithermal neutrons by ^{238}U. Due to the resonant peaks of the absorption cross section of this isotope and due to the chains of nuclear reactions that take place, several Pu isotopes are born especially at the rim. In particular, the fissile character of ^{239}Pu and ^{241}Pu is the cause of the increased number of fission events that occur in the pellet periphery. For this reason, the radial dependence of the power generation rate and the burnup accumulation needs to be considered. These parameters, which at low and intermediate burnup levels can be considered with a reasonably good approximation as uniformly distributed, reach values two or three times higher at the rim than at the rest of the pellet when the average burnup exceeds a certain magnitude [1].

A local burnup threshold value of about 60 MWd/kgHM can be established on an empirical basis for the initiation of the rim structure. This value of burnup in the pellet periphery is reached at an average burnup of 40–45 MWd/kgHM. Beyond this threshold, the width of the rim zone increases as the irradiation progresses. One of the distinctive features of the rim is its low thermal conductivity [1,2], which has a significant effect on the temperature distribution in the whole pellet. The size of grains and pores in the rim is markedly different to that in the fresh fuel. The new structure has an effect not only on the thermal conductivity, but also on the mechanical integrity of the pellet. The numerical codes designed to simulate fuel behavior under irradiation must include the phenomena associated with high burnup if they aim at extending the prediction range, and this is the purpose with our DIONISIO code. A detailed analysis of the aspects described above demands the formulation of the balance equations of all the isotopes that are born and destroyed during the irradiation process, taking into account the whole neutron energy range involved. This is a formidable task not suitable to be included in a fuel performance code, which must attend the great number of thermomechanical and thermochemical processes within the fuel rod.

The codes specialized in reactor physics perform these calculations, solving the Boltzmann transport equations [3] in a number of energy intervals (groups) and including adequate considerations in the region of the resonant absorption peaks of ^{238}U. They predict with high precision the radial distribution of neutron flux, burnup and concentration of every isotope, fissile, fissionable or fertile, gaseous or solid, within the rod, relevant for the overall process, all of them as functions of time. Among the known reactor codes, we mention WIMS-E [4,5], HELIOS [6,7], CONDOR [8], and HUEMUL [9].

In order to avoid the mentioned difficulties but without losing the required completeness, a simplified treatment was proposed in the past by reducing the energy spectrum to a single group. The purpose is to obtain empirical expressions to represent, with the higher possible approximation degree, the absorption, capture, and fission cross sections as functions of the initial enrichment in ^{235}U, the average burnup and the radial coordinate. The curves

* Corresponding author. Tel.: +54 11 6772 7241; fax: +54 11 6772 7345.
E-mail address: denis@cnea.gov.ar (A. Denis).

0022-3115/$ - see front matter © 2012 Elsevier B.V. All rights reserved.
http://dx.doi.org/10.1016/j.jnucmat.2012.08.016

obtained with a so drastic simplification demand a careful testing before incorporation into the general fuel behavior code. This testing is performed via comparison with the reliable reactor codes. After verification, the curves are incorporated into the fuel code, which is expected to give, with a reasonable precision, the time evolution of the local burnup and hence the size of the rim zone. The first antecedent in this type of analysis is found in the RADAR model [10], which was validated against the WIMS code. The TUBRNP model, included in the TRANSURANUS code [11] and the RAPID model [12], served as a basis for the development of the present work.

In this work, the original idea of RADAR is maintained, but the validity range and scope of the equations are extended. The curves fitted for the cross sections are compared with the predictions of the reactor cell codes HUEMUL and CONDOR. The final purpose is to extend the application range of the DIONISIO code [13–15] (originally designed to predict the fuel behavior in normal operation conditions) to the high burnup domain.

The HUEMUL code: The HUEMUL system is a two-dimensional cell code that calculates cross sections and simulates fuel burnup. It has a modular structure and solves the neutronic transport equation using the probability of collision theory. HUEMUL contains a basic scheme consisting of a number of elemental volumes called *representation mesh*. On this scheme, the calculation net is established, using the finite difference method, to give the neutron flux distribution and other neutronic parameters. In the representation mesh, the distribution of all fundamental properties of the system is defined: materials with the corresponding tables of cross sections, thermal–hydraulic properties, isotope concentrations, etc. All these parameters are stored in a data base and are available for any type of simulation.

The CONDOR code: The CONDOR calculation package uses a two dimensional Heterogeneous Response Method (HRM) [16] with angular dependent coupling currents to calculate the neutron flux distribution in fuel assemblies of nuclear reactor cores. In this method, whole fuel assembly is divided into cells or elements, which are coupled by interface currents. In each cell the calculations are performed by the collision probability method. Collision probabilities are numerically integrated using the Carlvik's method with a smart ray-tracing scheme, followed by normalization to reduce instabilities. Transformation laws on response fluxes and multiple collision escape and transmission probabilities are used to reduce the computational time. This method is applied not only during burnup but also when two elements with identical geometry have cross sections that differ very little. The CONDOR calculation package contains a library of nuclear data and works with a set of auxiliary programs. A distinctive feature of CONDOR is the use of the subgroups method which enables the simulation of the spatial shielding effect of the resonances.

With these codes, the time evolution of a fuel pellet was simulated. The final average burnup is given values ranging from fresh fuel to 120 MWd/kgHM. For enrichment, values in the interval from natural Uranium to 12% are assigned. The evolution of the radial distribution of ^{235}U, ^{236}U, ^{238}U, ^{239}Pu, ^{240}Pu, ^{241}Pu, and ^{242}Pu was obtained. These results were used to fit functions to represent the absorption and capture cross sections for each one of the above-mentioned species. A function to express the total flux as a function of the linear power, the enrichment, and the flux of thermal neutrons within the pellet was also fitted.

The present work describes the equations contained in the subroutine included in DIONISIO, the calculation methods used, and the empirical functions obtained. Two types of validations are presented: firstly, that referred to the comparison of the empirical expressions and the codes chosen as basis. Secondly, the results of numerous simulations performed with DIONISIO are presented and compared with the corresponding experimental data.

2. Numerical scheme

The balance equations considered in DIONISIO are listed below. They relate the variation rate of the concentration N (atoms/cm^3) of each of the relevant isotopes (indicated by subscripts formed by name of the element and mass number of the isotope) with the instantaneous value of the concentration. The cross section σ (expressed in barns) is labeled with a subscript a, c, or f to indicate absorption, capture or fission, respectively, and with a superscript to identify the nuclide. The same superscript is used to label the decay constant λ (measured in 1/s). ϕ (neutrons/(cm^2 s)) indicates the one-group neutron flux. N and ϕ are considered as functions of the irradiation time (t) and the radial position (r) in the pellet; σ is assumed to depend on the radius, the average burnup (b), and the initial enrichment (q) in ^{235}U measured in wt.%.

$$\frac{\partial N_{U235}}{\partial t} = -N_{U235}(t,r)\sigma_a^{235}(r,b,q)\phi(t,r) \tag{1}$$

$$\frac{\partial N_{U236}}{\partial t} = -N_{U236}(t,r)\sigma_a^{236}(r,b,q)\phi(t,r) + N_{U235}(t,r)\sigma_c^{235}(r,b,q)\phi(t,r) \tag{2}$$

$$\frac{\partial N_{U238}}{\partial t} = -N_{U238}(t,r)\sigma_a^{238}(r,b,q)\phi(t,r) \tag{3}$$

$$\frac{\partial N_{Pu239}}{\partial t} = -N_{Pu239}(t,r)(\sigma_a^{239}(r,b,q)\phi(t,r) + \lambda^{239}) + N_{U238}(t,r)\sigma_c^{238}(r,b,q)\phi(t,r) \tag{4}$$

$$\frac{\partial N_{Pu240}}{\partial t} = -N_{Pu240}(t,r)(\sigma_a^{240}(r,b,q)\phi(t,r) + \lambda^{240}) + N_{Pu239}(t,r)\sigma_c^{239}(r,b,q)\phi(t,r) \tag{5}$$

$$\frac{\partial N_{Pu241}}{\partial t} = -N_{Pu241}(t,r)(\sigma_a^{241}(r,b,q)\phi(t,r) + \lambda^{241}) + N_{Pu240}(t,r)\sigma_c^{240}(r,b,q)\phi(t,r) \tag{6}$$

$$\frac{\partial N_{Pu242}}{\partial t} = -N_{Pu242}(t,r)(\sigma_a^{242}(r,b,q)\phi(t,r) + \lambda^{242}) + N_{Pu241}(t,r)\sigma_c^{241}(r,b,q)\phi(t,r) \tag{7}$$

Reactor codes generally divide the neutrons' energy spectrum in two groups, described as *thermal* (neutrons with energies below 0.65 eV) and *fast* (neutrons with higher energies).

To determine the total neutron flux, a parametric expression is built in terms of the initial enrichment, the average burnup, and the linear power in the pellet.

$$\phi_{tot} = \frac{P_{vol}}{3.2\times10^{-11}}\frac{1}{\sum_i \sigma_f^i(r,b,q)\langle N_i\rangle} \tag{8}$$

where P_{vol} is the volumetric power density expressed in W cm^{-3}. This function is compared with the predictions of HUEMUL and CONDOR, assuming typical conditions of a PWR reactor.

The total flux is used in the balance Eqs. (1)–(7) to predict the behavior of each isotope.

The cross section functions to be introduced in the subroutine are evaluated as follows: the codes CONDOR and HUEMUL are run assuming the conditions of a generic UO_2 pellet; the initial enrichment is varied from 0.7% to 12%; the final average burnup is given values ranging from fresh fuel to 120 MWd/kgU. With these results, empirical expressions are fitted for the absorption, capture and fission cross sections of each relevant isotope, neutron flux and local burnup, all of them as functions of the radial

coordinate (r), the average burnup (b) and the enrichment (q). In this way, the so-generated expressions are valid in a continuous range limited by the extreme values of the parameters r, b, and q. The empirical correlations that we indicate as $\sigma^{i}_{a,c,f}$ for absorption, capture or fission of the nuclide i, are introduced in DIONISIO and subjected to several tests: firstly, the parameterized functions are compared with the curves obtained with the reactor codes; secondly, the predictions of the balance Eqs. (1)–(8) are compared with those of the reactor physics codes; and finally, the empirical expressions are introduced in DIONISIO, and the predictive ability of the code as a whole is tested by comparison of its results with experimental data.

The formulae fitted in the present work for the cross sections of absorption, capture and fission of ^{235}U, ^{236}U, ^{238}U, ^{239}Pu, ^{240}Pu,

Table 1
Correlation formulae and the corresponding coefficients for the fission cross section of ^{235}U, the absorption cross sections of ^{238}U, ^{239}Pu and ^{241}Pu, and the total neutron flux, calculated for a single energy group.

$\sigma_f^{235} = f_1(r,b,q)$ Eq. (9), with
$a_0 = 7.5185 \times 10^{1} - 3.3072 \times 10^{1}q + 7.4396q^2 - 8.3136 \times 10^{-1}q^3 + 3.5577 \times 10^{-2}q^4$
$a_1 = 9.0481 + 7.111q$
$a_2 = -2.9476 \times 10^{-3} + 1.882 \times 10^{-3}q - 5.0146 \times 10^{-4}q^2 + 6.024 \times 10^{-5}q^3 - 2.677 \times 10^{-6}q^4$
$a_3 = -2.792 \times 10^{1} - 2.6119 \times 10^{1}q$
$a_4 = -3.0152 \times 10^{-5} - 2.8059 \times 10^{-5}q + 2.4603 \times 10^{-5}q^2 - 3.8561 \times 10^{-6}q^3 + 1.8424 \times 10^{-7}q^4$
$a_5 = 4.5631 \times 10^{-8} - 3.0459 \times 10^{-8}q + 8.3540 \times 10^{-9}q^2 - 1.0234 \times 10^{-9}q^3 + 4.609 \times 10^{-11}q^4$
$a_6 = 5.4365 \times 10^{1} + 2.8356 \times 10^{1}q$
$a_7 = -4.8075 \times 10^{-5} - 5.0176 \times 10^{-5}q - 3.111 \times 10^{-7}q^2 + 1.0188 \times 10^{-6}q^3 - 6.2605 \times 10^{-8}q^4$
$a_8 = 4.4372 \times 10^{-10} + 4.0461 \times 10^{-10}q - 1.7849 \times 10^{-10}q^2 + 2.4625 \times 10^{-11}q^3 - 1.1431 \times 10^{-12}q^4$
$a_9 = -2.1647 \times 10^{-13} + 1.4578 \times 10^{-13}q - 4.0347 \times 10^{-14}q^2 + 4.9812 \times 10^{-15}q^3 - 2.2566 \times 10^{-16}q^4$

$\sigma_a^{238} = f_2(r,b,q)$ Eq. (10), with
$a_0 = 1.10 - 0.011q$
$a_1 = 0.90$
$a_2 = 1.21 \times 10^{-6}$
$a_3 = -8.030 \times 10^{-14}$
$a_4 = -1.32 \times 10^{-17}$
$a_5 = 0.920$
$a_6 = 6.50 + 0.069q$
$a_7 = -8.760$
$a_8 = 0.389$

$\sigma_f^{238} = f_1(r,b,q)$ Eq. (9), with
$a_0 = 8.1519 \times 10^{-2} + 2.6563 \times 10^{-3}q$
$a_1 = 8.37631 \times 10^{-3} + 5.0092 \times 10^{-4}q$
$a_2 = 4.1793 \times 10^{-7} - 1.2974 \times 10^{-7}q + 9.8303 \times 10^{-9}q^2$
$a_3 = -2.1242 \times 10^{-2} - 1.1110 \times 10^{-3}q$
$a_4 = 0$
$a_5 = -3.4248 \times 10^{-12} + 2.1605 \times 10^{-12}q - 5.3806 \times 10^{-13}q^2 + 6.1105 \times 10^{-14}q^3 - 2.6081 \times 10^{-15}q^4$
$a_6 = a_7 = a_8 = a_9 = 0$

$\sigma_a^{239} = f_1(r,b,q)$Eq. (9), with
$a_0 = 3.5660 \times 10^{2} - 1.1991 \times 10^{2}q + 2.2334 \times 10^{1}q^2 - 2.0188q^3 + 6.8935 \times 10^{-2}q^4$
$a_1 = 5.1434 \times 10^{1} + 1.4796q$
$a_2 = -3.1433 \times 10^{-3} + 9.2646 \times 10^{-4}q - 1.2357 \times 10^{-4}q^2 + 5.6483 \times 10^{-6}q^3$
$a_3 = -2.3028 \times 10^{2} - 7.7734q$
$a_4 = 2.6476 \times 10^{-4} - 1.0885 \times 10^{-4}q + 3.8593 \times 10^{-5}q^2 - 4.3834 \times 10^{-6}q^3 + 1.5858 \times 10^{-7}q^4$
$a_5 = 4.7940 \times 10^{-8} - 2.6188 \times 10^{-8}q + 7.1850 \times 10^{-9}q^2 - 7.9332 \times 10^{10}q^3 + 2.9875 \times 10^{-11}q^4$
$a_6 = 4.3017 \times 10^{2} + 1.0274 \times 10^{1}q$
$a_7 = -2.9149 \times 10^{-4} + 3.9603 \times 10^{-4}q - 1.2326 \times 10^{-4}q^2 + 1.4558 \times 10^{-5}q^3 - 5.7856 \times 10^{-7}q^4$
$a_8 = -6.7461 \times 10^{-10} - 6.6462 \times 10^{-10}q + 1.6253 \times 10^{-10}q^2 - 1.9151 \times 10^{-11}q^3 + 8.4808 \times 10^{-13}q^4$
$a_9 = -1.8470 \times 10^{-13} + 1.1543 \times 10^{-13}q - 3.4986 \times 10^{-14}q^2 + 4.1371 \times 10^{-15}q^3 - 1.6382 \times 10^{-16}q^4$

$\sigma_a^{241} = f_1(r,b,q)$,Eq. (9), with
$a_0 = 2.4628 \times 10^{2} - 4.1349 \times 10^{1}q + 2.2182q^2$
$a_1 = 4.2627 \times 10^{1} + 1.2053q$
$a_2 = -2.7869 \times 10^{-3} + 1.0306 \times 10^{-3}q - 1.4692 \times 10^{-4}q^2 + 6.8534 \times 10^{-6}q^3$
$a_3 = -1.8472 \times 10^{2} - 6.9921q$
$a_4 = 1.4759 \times 10^{-4} - 1.0087 \times 10^{-4}q + 3.6526 \times 10^{-5}q^2 - 4.1962 \times 10^{-6}q^3 + 1.5673 \times 10^{-7}q^4$
$a_5 = 4.6317 \times 10^{-8} - 3.0198 \times 10^{-8}q + 8.4079 \times 10^{-9}q^2 - 9.2821 \times 10^{-10}q^3 + 3.5034 \times 10^{-11}q^4$
$a_6 = 3.6782 \times 10^{2} + 8.4903q$
$a_7 = -1.7106 \times 10^{-4} + 1.5232 \times 10^{-4}q - 5.4102 \times 10^{-6}q^2 + 6.8122 \times 10^{-6}q^3 - 2.7941 \times 10^{-7}q^4$
$a_8 = -2.8419 \times 10^{-10} + 7.3795 \times 10^{-11}q - 3.6610 \times 10^{-11}q^2 + 2.5256 \times 10^{-12}q^3$
$a_9 = -5.1539 \times 10^{-14} + 9.6817 \times 10^{-15}q - 3.0403 \times 10^{-15}q^2 + 2.3750 \times 10^{-16}q^3$

$\phi_{total} = f_3(r,b,q)$ Eq. (11), with
$a_0 = 0.700$
$a_1 = -3.0432 \times 10^{-9}$
$a_2 = 0.0113$
$a_3 = 3.5805 \times 10^{-17}$
$a_4 = 5.2119 \times 10^{-11}$
$a_5 = -0.0013$
$a_6 = -1.1270 \times 10^{-25}$
$a_7 = -1.6796 \times 10^{-18}$
$a_8 = 1.3674 \times 10^{-11}$
$a_9 = 2.7321 \times 10^{-5}$

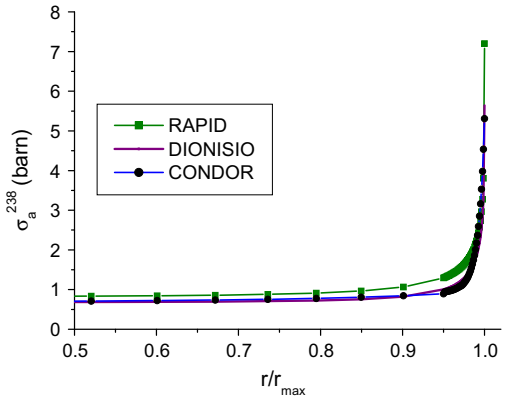

Fig. 1. Comparison between the results obtained with the correlation law developed in DIONISIO for the absorption cross section of ^{238}U and the results given by RAPID and CONDOR. The example corresponds to a pellet with an initial enrichment of 3 w% in ^{235}U and an average burnup of 58 MWd/kgU.

^{241}Pu and ^{242}Pu and for the total neutron flux can be grouped in the following function shapes:

$$f_1(r,b,q) = a_0 + a_1 r + a_2 b + a_3 r^2 + a_4 rb + a_5 b^2 + a_6 r^3 + a_7 r^2 b + a_8 rb^2 + a_9 b^3 \quad (9)$$

$$f_2(r,b,q) = a_0(a_1 + a_2 b + a_3 b^2 + a_4 b^3)\left(a_5 + a_6 \exp\left(a_7\left(1 - \frac{r}{r_{max}}\right)^{a_8}\right)\right) \quad (10)$$

$$f_3(r,b,q) = \frac{P_{vol}}{3.2 \times 10^{-11} \sum_i \sigma_f^i(r,0,1) N_i} \cdot (a_0 + a_1 b + a_2 q + a_3 b^2 + a_4 bq + a_5 q^2 + a_6 b^3 + a_7 b^2 q + a_8 bq^2 + a_9 q^3) \quad (11)$$

where σ_f^i (r,0,1) represents the fission cross section of isotope i in the reference condition corresponding to fresh fuel ($b = 0$) and enrichment 1 wt% ($q = 1$).

In the election of the coefficients, the criterion was to optimize the fitting in the intermediate ranges of burnup and/or initial enrichment, that is, from 20 to 80 MWd/kgHM and from 3 to 8 w% ^{235}U, respectively, since these are the values of interest in the present fuel development studies.

3. Results

By way of example, the empirical expressions obtained for σ_f^{235}, σ_a^{238}, σ_a^{239}, and σ_a^{241} (representing the fission cross section of ^{235}U and the absorption cross sections of ^{238}U, ^{239}Pu and ^{241}Pu, respectively) and those for ϕ_{tot} are displayed in Table 1. Similar correlations, not listed in the Table, were obtained for the rest of the cross sections used in the equations system (1)–(7).

These correlations represent surfaces in a four-dimensional space defined by the variables r, b, q, and σ or ϕ. Figs. 1–3 show some particular sections of these surfaces. They make evident the good quality of the approximations obtained with the correlations determined in the present work in comparison with the results given by reliable reactor codes like RAPID, CONDOR, and HUEMUL. The selected examples correspond to the absorption cross section σ_a^{238} of ^{238}U, the fission cross section σ_f^{239} of ^{239}Pu, and the

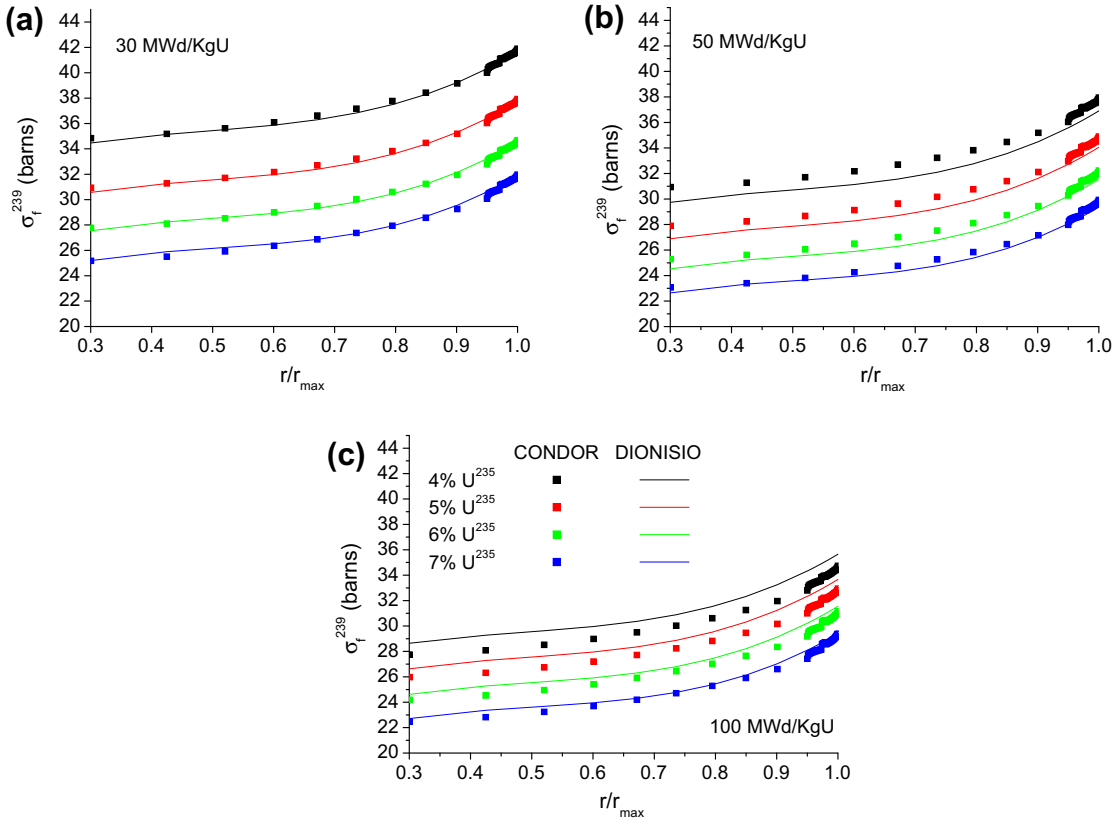

Fig. 2. Fission cross section σ_f^{239} of ^{239}Pu vs. the relative radius for different values of the initial enrichment and different levels of average burnup. Comparison between the values predicted by CONDOR and the functions included in DIONISIO. The legend in (c) applies for the three plots.

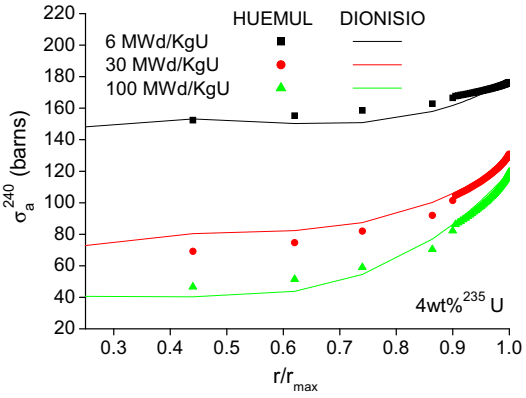

Fig. 3. Absorption cross section σ_a^{240} of ^{240}Pu vs. the relative radius for an initial enrichment of 4 wt% in ^{235}U and different levels of average burnup. Comparison between the values predicted by HUEMUL and the functions included in DIONISIO.

absorption cross section σ_a^{240} of ^{240}Pu, respectively, vs. the relative radius for different values of the initial enrichment and different levels of average burnup.

The first of them deserves special attention. The depletion of Uranium that is observed in the external pellet zone is basically due to the behavior in the resonance region of the absorption cross section of Uranium 238. The effective absorption cross section evaluated by CONDOR, RAPID, and DIONISIO is represented in Fig. 1 vs. the relative radius of the pellet. The calculations were performed for typical, representative values of enrichment and average burnup.

Given that the cross sections are functions of several variables, different intersections can be taken. For instance, in each plot of Fig. 2, a fixed value of average burnup has been chosen and several curves have been drawn for different enrichments. In contrast, in Fig. 3, the initial enrichment is fixed and the curves are plotted for different values of the average burnup.

Fig. 4 shows the concentration in atoms/cm^3 of the relevant Pu isotopes. The curves correspond to the time evolution at the pellet mean radius. Each plot was drawn for a given initial enrichment. As in Figs. 2 and 3, the solid lines represent the simulations of DIONISIO and the dotted lines the results given by HUEMUL.

The local burnup, obtained as the result of the contributions of all the fissile isotopes, is plotted in Fig. 5 as a function of the radius. Each curve has been drawn for a given value of the average burnup. In this example, the results of DIONISIO are compared with those of CONDOR.

4. Validation with experimental results

Experimental data corresponding to the high burnup range were chosen from the NEA data bank to compare the code results with.

In particular, experimental determinations of the total U and Pu content are found in the IFA-597 report. In this experiment, a Westinghouse Atom 8 × 8 fuel rod irradiated in the Ringhals 1 BWR for 12 years to an average burnup of about 68 MWd/kgU was refabricated, instrumented with centreline thermocouple and pressure transducer, and irradiated for about 1 month at a rod-average linear heat rate in the range 25–20 kW/m. Then, several post-irradiation examinations were performed [17]: punctur-

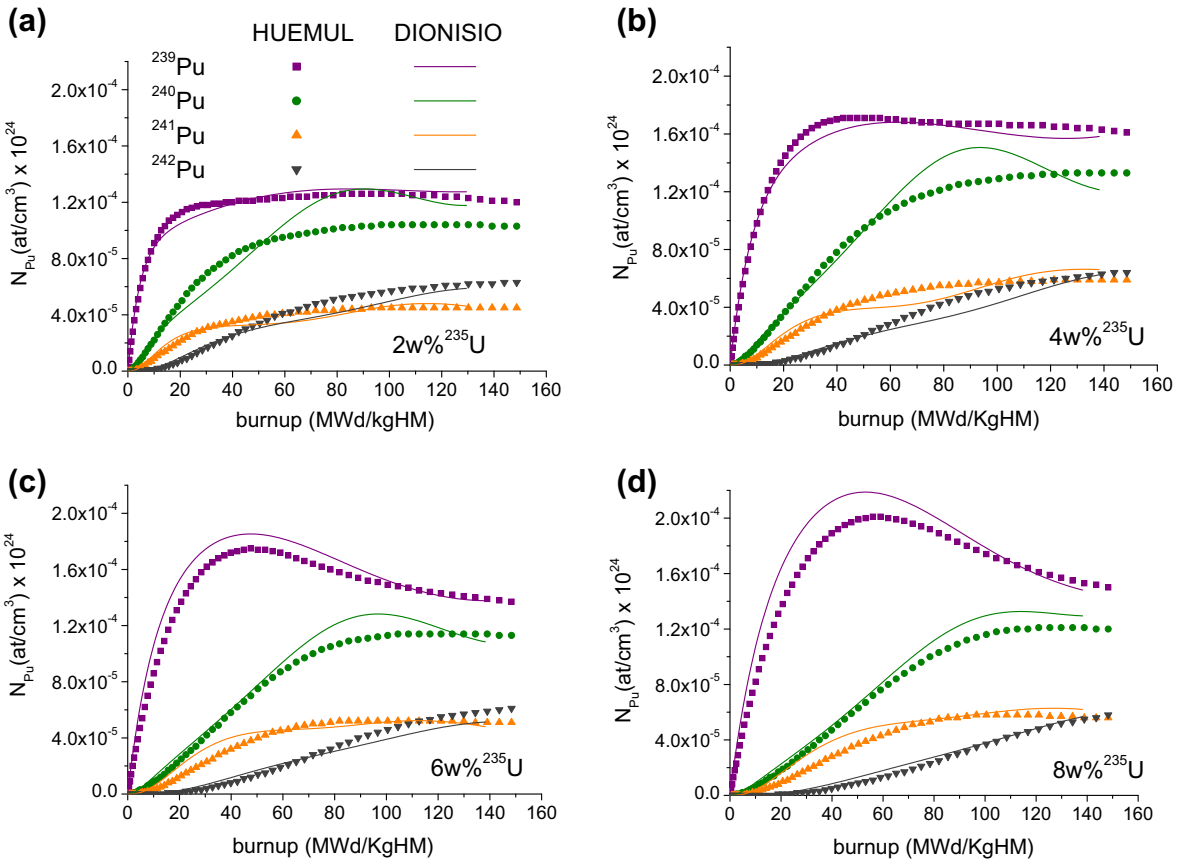

Fig. 4. Concentration of ^{239}Pu, ^{240}Pu, ^{241}Pu and ^{242}Pu vs. burnup for different values of the initial enrichment, predicted by HUEMUL and DIONISIO, for $r/r_{max} \approx 0.5$. The legend in (a) applies for the four plots.

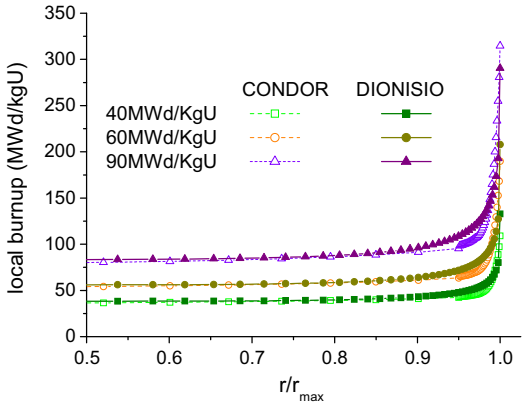

Fig. 5. Comparison between the distribution of burnup obtained with the correlation laws developed in DIONISIO and the results given by CONDOR, for different levels of average burnup.

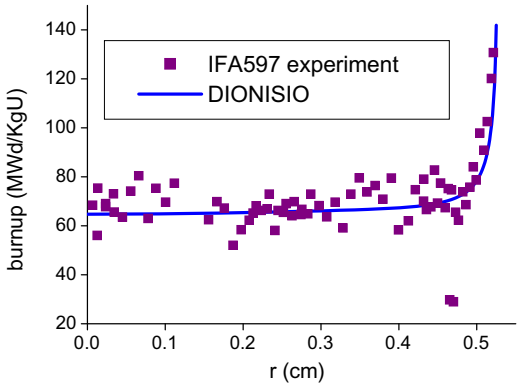

Fig. 7. Experimental and simulated radial burnup profile within the pellet.

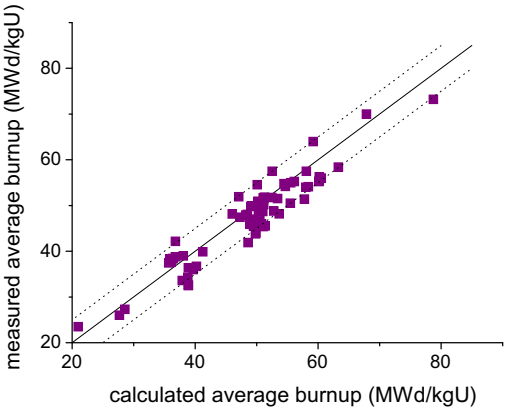

Fig. 8. Comparison between calculated and measured values of the average burnup.

ing followed by mass spectrometry, EPMA, optical and scanning electron microscopy, profilometry, among others. In particular, EPMA is used to determine the local concentration of U, Pu, Ce, and several other elements.

Fig. 6 shows the experimental values and the simulation results of the radial distribution of the total Plutonium ($N_{Pu239}+N_{Pu240}+N_{Pu241}+N_{Pu242}$) and Uranium ($N_{U235}+N_{U236}+N_{U238}$) content in the pellet. In spite of the important scatter of the experimental values, it is seen that the simulation gives a reasonable average value of the measured quantities of both elements.

The experimental values of local burnup are obtained in IFA 597 from the determinations of Ce. They are shown in Fig. 7 along with the results calculated with DIONISIO. Both give an average burnup of 72 MWd/kgU. In the rim, a maximum burnup of 131 MWd/kgU is experimentally estimated while the code predicts about 141 MWd/kgU. The agreement is remarkably good, especially if we take into account that the experimental technique employed underestimates the actual burnup in the rim by a 10–20%, as assessed in ref [17].

An important set of experiments gives origin to the comparisons presented in Figs. 8 and 9. They take part of the FUMEX II [18] and III [19] data basis. In particular, the values of average burnup simulated with DIONISIO are compared in Fig. 8 with the data obtained in the experiments HBEP-R1–3 [20], US PWR-103 [21], Tribulation [22], Spc-re-ginna [23,24], Risoe 3 [25], Osiris [26–28], Kola-3 [29,30], Gain [31], and IFA [17]. The mean value of the absolute difference between calculated and measured values represents 6.2% of the mean value of the experimental data. All the points in Fig. 8 fall within the range ±5 MWd/kgU (indicated in the figure with the dotted parallel lines) around the solid line that represents perfect agreement between calculations and measurements.

Similarly, Fig. 9 shows the comparison between calculated and measured values of total Plutonium content corresponding to experiments HBEP-3 [20], Regate [32], Riso-GE [25], Osiris-G07/H09 [27,28]. The plot, that involves about 500 data, reveals a good agreement between the calculated and measured values since 98% of the points fall within the range ±0.5 wt.%, represented in the figure with the dotted parallel lines, around the line of perfect agreement. With reference to same set of points, the mean value of the absolute difference between calculated and measured values

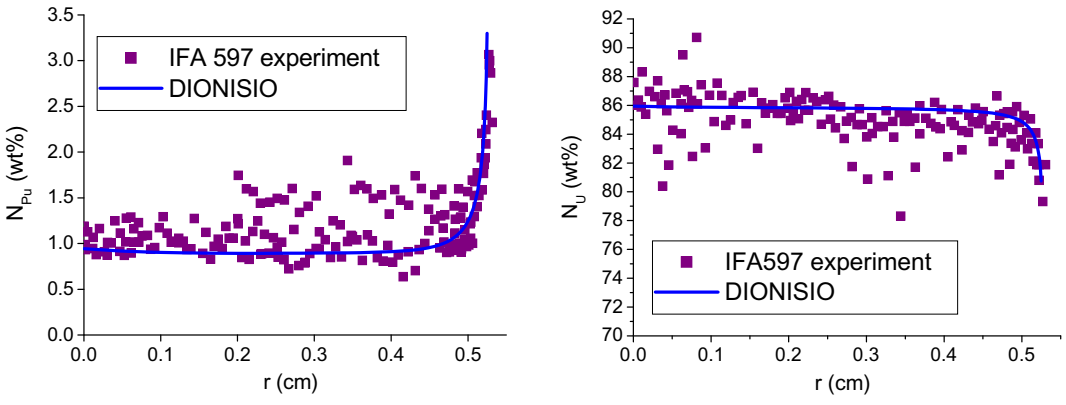

Fig. 6. Total Plutonium and Uranium concentration vs. the radial position in the pellet.

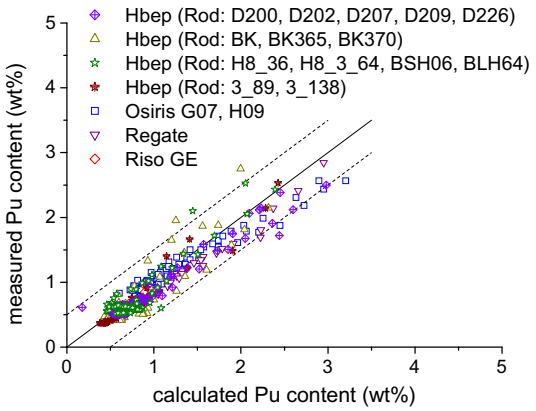

Fig. 9. Comparison between calculated and measured values of total Pu content.

represents 15.4% of the mean value of the measured data, expressing also the good quality of the approximation reached with the simulations.

5. Conclusions

A subroutine designed to predict the effects of high burnup on the fuel pellet has been recently developed and included in the DIONISIO code. It calculates the radial profiles of the more significant Uranium and Plutonium isotopes. The localized absorption of epithermal neutrons by ^{238}U, with all the consequences it entails, is assumed to be responsible for the formation of the rim structure.

Before the incorporation of this subroutine to DIONISIO, the simulation range of the code was limited to average burnup levels below 40–45 MWd/kgHM (i.e., prior to the appearance of the high burnup microstructure). In its present version, the code gives reasonably accurate results for average burnup levels of 120 MWd/kgHM, which correspond to local values in the pellet edge as high as 300 MWd/kgHM. A necessarily simplified calculation scheme is adopted consisting of reducing the energy spectrum to a single group. Even though the approximation is quite drastic, the agreement with the results given by reliable neutronic codes is good, as revealed by the comparisons presented in this work. In particular, the curves obtained with the simplified scheme for the absorption cross section of ^{238}U and the distribution of burnup as functions of the radial position within the pellet (Fig. 1 are Fig. 5, respectively) have not only the expected shape but also in perfect agreement with those obtained with the neutronic calculation tools. This work also presents the comparison between experimental data provided by the IAEA (in particular those collected in the FUMEX II and III data basis) and the simulations of DIONISIO, which revealed a very good agreement.

Acknowledgement

The authors acknowledge the important suggestions and advices of Carlos Grant during the preparation of this paper.

References

[1] Hj. Matzke, J. Nucl. Mater. 189 (1992) 141–148.
[2] M.E. Cunningham, M.D. Freshley, D.D. Lanning, J. Nucl. Mater. 188 (1992) 19–27.
[3] S. Glasstone, A. Sesonske, in: S.A. Reverté (Ed.), Ingenieria de reactores nucleares, Buenos Aires, 1975.
[4] T.D. Newton, J.L. Hutton, in: M.G. Park (Ed.), Proceedings of PHYSOR 2002 – International Conference on the New Frontiers of Nuclear Technology: Reactor Physics, Safety and High-Performance Computing, 14A-04, American Nuclear Society, Seoul, Korea, 2002, pp. 7–10.
[5] J.L. Hutton, T.D. Newton, R.J. Perry, D.J. Powney, in: Proceedings of PHYSOR 2004 – The Physics of Fuel Cycles and Advanced Nuclear Systems: Global Developments, Session 1D, American Nuclear Society, Chicago, Illinois, USA, 25–29 April 2004.
[6] R.J.J. Stammler, S. Boerresen, J.J. Casal, P. Forslund, in: Proceedings of PHYSOR 1996 – International Conference on Physics of Reactors, American Nuclear Society, Mito, Ibaraki, Japan, 16–20 September 1996.
[7] HELIOS Methods, Program Manual Rev. 1, Program HELIOS 1.4, Studsvik-Scandpower, 1998.
[8] E. Villarino, Condor Calculation Package PHYSOR 2002, Seoul, Korea, 2002, pp. 7–10.
[9] C. Grant, personal communication.
[10] I.D. Palmer, K.W. Hesketh, P.A. Jackson, in: J. Gittus (Ed.), Water Reactor Fuel Element Performance Computer Modelling, Applied Science, Barking, UK, 1983, p. 321.
[11] A. Schubert, P. Van Uffelen, J. van de Laar, C.T. Walker, W. Haeck, J. Nucl. Mater. 376 (2008) 1–10.
[12] Chan Bock Lee, Dae Ho Kim, Jae Seung Song, Je Gun Bang, Youn Ho Jung, J. Nucl. Mater. 282 (2000) 196–204.
[13] Simulación del comportamiento termomecánico de una barra combustible en operación, Alejandro Soba. Tesis de doctorado, FCEyN, UBA, 2007.
[14] A. Denis, A. Soba, Nucl. Eng. Des. 223 (2003) 211–229.
[15] A. Soba, A. Denis, J. Nucl. Mater. 374 (2008) 32–43.
[16] E. Villarino, R. Stamm'ler, A. Ferri, J. Casal, Nucl. Sci. Eng. 112 (1992).
[17] K. Malén, A. Micski, D. Schrire, B. Nilsson, PIE of high burnup BWR fuel rod IFA-597.3 (ROD 8), Studsvik Nuclear AB SwedenHRP-356/U.
[18] NEA-1510 IFPE/HBEP-3 REV.1 - High Burnup Effects Programme Final Report, DOE/NE/34046-1 [HBEP-61(3P27)].
[19] J. Killeen, E. Sartori, T. Tverberg, FUMEX-III: A new IAEA coordinated research project on fuel modelling at extended burnup. Top Fuel 2009, 2009.
[20] W.F. Lyon, US-PWR 16 × 16 LTA Extended Burnup Demonstration Program Summary File, 2005.
[21] NEA-1738 IFPE/US-PWR-16 × 16LTA.
[22] NEA-1536 IFPE/TRIBULATION R1.
[23] IFPE/SPC-RE-GINNA NEA-1623/01.
[24] SPC-re-ginna G.A. Sofer and L.F.P. van Swam: Annular-Pellet Barrier-Clad Fuel Assemblies at the R.E. Ginna PWR: Hotcell Examinations EP 80-17 Final Report, vol. 1, 1997.
[25] IFPE/RISOEIII, NEA-1493/17.
[26] IFPE/OSIRIS, NEA-1622/04.
[27] Rapport d'Assurance Qualite Crayon FF06E2BV/G07/1067.
[28] Rapport d'Assurance Qualite Crayon FF0EFELX/H09/5007.
[29] IFPE/KOLA-3-MIR-RAMP, NEA-1766/02.
[30] Smirnov, B. Kanashov, V. Kuzmin, et al., Results of post irradiation examinations to validate WWER-440 and WWER-1000 fuel efficiency at high burnup, in: Proceedings of the Third International Seminar WWER Fuel Performance, Modelling and Experimental Support, Varna, Bulgaria, 2001, pp. 1–5.
[31] NEA-1625 IFPE/GAIN.
[32] NEA-1696 IFPE/REGATE L10.3.